

# Soccer line mark segmentation and classification with stochastic watershed transform

Daniel Berjón<sup>a</sup>, Carlos Cuevas<sup>a</sup>, Narciso García<sup>a</sup>

<sup>a</sup>*Information Processing and Telecommunications Center — Universidad Politécnica de Madrid, Av. Complutense, 30, Madrid, 28029, Spain*

---

## Abstract

Augmented reality applications are beginning to change the way sports are broadcast, providing richer experiences and valuable insights to fans. The first step of augmented reality systems is camera calibration, possibly based on detecting the line markings of the playing field. Most existing proposals for line detection rely on edge detection and Hough transform, but radial distortion and extraneous edges cause inaccurate or spurious detections of line markings. We propose a novel strategy to automatically and accurately segment and classify line markings. First, line points are segmented thanks to a stochastic watershed transform that is robust to radial distortions, since it makes no assumptions about line straightness, and is unaffected by the presence of players or the ball. The line points are then linked to primitive structures (straight lines and ellipses) thanks to a very efficient procedure that makes no assumptions about the number of primitives that appear in each image. The strategy has been tested on a new and public database composed by 60 annotated images from matches in five stadiums. The results obtained have proven that the proposed strategy is more robust and accurate than existing approaches, achieving successful line mark detection even in challenging conditions.

*Keywords:* segmentation, watershed, soccer, classification, line mark

---

## 1. Introduction

Soccer is the most popular sport in the world, not only in terms of television audience (almost 4 billion followers in 200 countries) or players (more than 260 million) [1], but also regarding research [2]. Much of the research work proposed in recent years has focused on responding to the demand for applications capable of enriching the content of live broadcasts with augmented reality [3] and applications aimed at analyzing and understanding the game [4, 5].

To tackle these high-level tasks, it is required to register the images in a model of the playing field [6] and/or calibrate the cameras [7, 8]. The strategies with these aims are typically based on the detection of key-points determined from the intersections between the line marks on the grass [9]. These line marks can be of two types, straight lines and circles (seen as ellipses in the images). Therefore, the location of the line marks is a key stage in all these high-level tasks. However, existing methods exhibit shortcomings in difficult

lighting conditions, require manual tuning or rely on assumptions about the straightness or distribution of line markings.

In this paper we propose a novel method to detect the playing field line points and determine which of them belong to straight lines and which to ellipses. The quality of the results obtained has been assessed in a database composed of numerous annotated images taken from a wide variety of points of view, in different and challenging lighting conditions, and its usefulness has been demonstrated after being compared with other state-of-the-art methods. Although we focus on soccer videos, the proposed strategy can be adapted to other types of “pitch sports”.

### *1.1. Contribution*

The main contributions of this work are:

- Line mark segmentation using a stochastic watershed transformation. Many proposals for line marking detection start from a proto-edge-detection stage that yields many unwanted or duplicate edges. Unlike existing methods, we use the watershed transformation because it lends itself naturally to flood out irrelevant edges such as those due to the players or the ball.
- Seed placing strategy. Our proposal builds upon the stochastic watershed algorithm [10], but our goal is different (line marking detection instead of region segmentation); hence, our method does not require the user to manually set a number of relevant regions to be sought and ensures quick convergence.
- Viewpoint-independent classification of line marks into the two kinds of primitive structures that appear in soccer fields: straight lines and ellipses. Previous works apply independent algorithms to detect straight lines and ellipses, while we perform a joint analysis that provides higher quality results. Additionally, unlike those works, we not only detect the center circle but also the penalty arcs.

### *1.2. Organization*

The paper is organized as follows: in section 2 we review existing algorithms for line marking detection. Sections 3 and 4 describe our proposal for line mark segmentation and classification, respectively. Experiment results are reported in section 5 and, finally, section 6 presents the conclusions of the paper.

## **2. Related work**

To measure distances and speeds of players and/or ball throughout the matches, the images need to be registered to a model of the playing field. This is typically accomplished from sets of key-points that result from intersections between line marks.

To bring out the white line marks from the rest of the elements in the playing field, some authors use edge detectors: the Sobel detector in [11, 12], the Canny detector in [13, 14], or the Laplacian of Gaussian (LoG) detector in [15, 16]. To obtain the points centered in the

line marks, other authors use the Top-Hat transform [6, 17, 18]. There are also works that apply combinations of morphological operations [19]. All these methods, although quick and simple, have the important drawback of the correct selection of a threshold. If the threshold value is too high, they are not able to detect the lines in the lower contrast areas of the image (heavily shadowed or brightly lit areas). On the other hand, if the threshold is too low, numerous false detections occur due to the grass texture and the presence of players on the pitch.

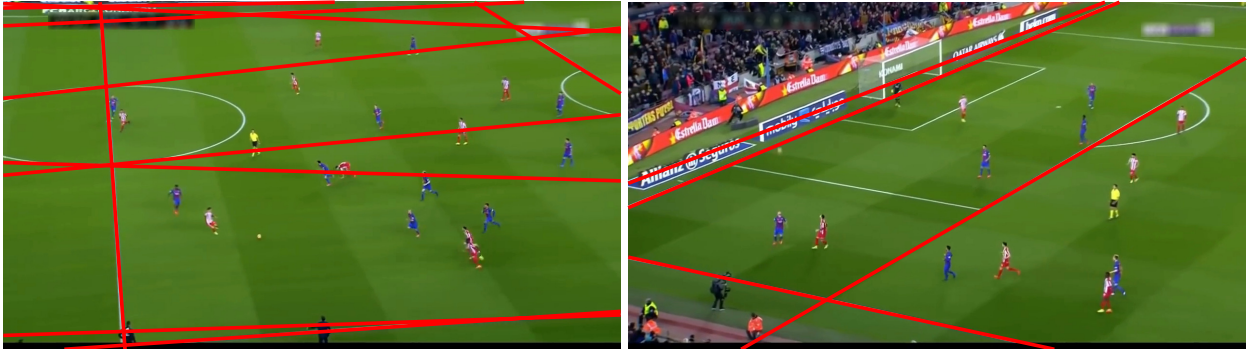


Figure 1: Examples of typical line mark detections using the Hough transform superimposed on the original images.

Once the white lines mask is obtained, most strategies apply the Hough transform to detect the straight line marks [9]. The Hough transform is computationally efficient and provides successful results in simple images. However, it is very sensitive to the presence of the aforementioned false detections and therefore results in numerous false lines. An additional drawback of Hough-based methods is the need to set the number of lines to consider. Typically, in images captured by the Master Camera<sup>1</sup>, the maximum number of straight lines that can be seen is 10 (straight lines on each of the halves of the playing field). However, in many cases significantly fewer lines are visible. If the number of lines considered is too high, in images showing few straight lines several false detections are obtained (see left image in Fig. 1). On the other hand, if the number of lines considered is too low, in images with many lines (e.g., images showing any of the goal areas), some lines are misdetections (see right image in Fig. 1). To reduce these misdetections, some works have proposed the application of the Hough transform independently along small windows that cover the entire image [20]. A further drawback of Hough-based methods is that the images generally suffer from radial distortion. Consequently, duplicate lines are typically obtained (see the bottom line shown in the left image in Fig. 1).

Once the straight lines have been detected, they are typically classified according to their tilt [6, 21]. However these analyses are limited to the cases in which the position of

<sup>1</sup>The master camera is the one used most of the time in soccer broadcasting and also the only one considered in most approaches in the literature. It is placed approximately on the extension of the halfway line. It performs pan, tilt, and zoom movements, but not rotations around its longitudinal axis (i.e., no roll).

the camera used to acquire the images is known [22]. Alternatively, the lines are classified in only two sets (longitudinal and transverse) that are used to determine two vanishing points [23, 24].

There are also strategies that focus on detecting the center circle of the playing field [19]. Some of them use a 6-dimensional Hough transform to detect ellipses [25] since, due to the perspective of the images, the center circle is seen as an ellipse in the images. These strategies have very high computational and memory requirements [26, 27]. Additionally, since the Hough transform is applied on edge or Top-Hat images, their results are inaccurate because of the presence of players, billboards, etc. An additional limitation of these algorithms is that they cannot obtain successful results in images where the center circle does not appear complete. Alternatively, some authors have proposed strategies using Least Squares Fitting (LSF) methods [28]. However, since they are also very sensitive to the presence of data that do not belong to the ellipse [29], they require complex steps to discard data from other lines, players, etc [6]. Another important limitation of all these strategies is that none of them is able to detect the circles of the penalty areas.

### 3. Watershed-based line mark segmentation

We propose a completely automatic procedure based on stochastic watershed [10, 30] to detect the line markings in a soccer pitch. The usual purpose of a watershed transform is to segment regions in a grayscale image separated by higher ground [31], interpreting the levels of the image as terrain elevation. However, since every local minimum is such a region, the user has to manually determine how many significant regions are there in the image, and even small discontinuities in the ridges between regions can upset the results (see Fig. 2).

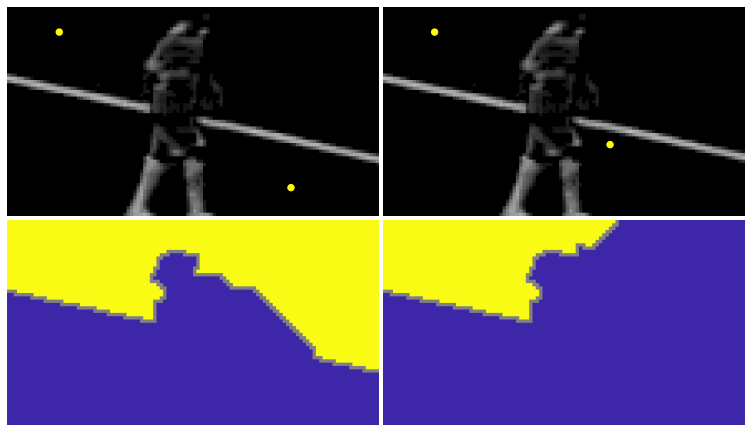


Figure 2: Examples of different segmentation results (bottom) depending on the position of the seeds (top). Note that although a human observer interprets as clearly distinct areas those above and below the line marking, they are actually joined due to the interference of the player.

In our case, however, we are not interested in the regions themselves but in the lines that delimit them, and we do not care if a discontinuity in a line as the one shown in Fig. 2 joins two regions. The basic idea is that, since the line markings are brighter than their

surroundings, if we manage to place *numerous* markers well distributed throughout both sides of every line mark, the result will be an image whose watershed lines will include (almost) every portion of the line markings we want to detect, along with a lot of spurious lines due to having placed many more markers than there are regions. However, upon repetition of the experiment with different sets of markers, spurious lines will change, as illustrated in Fig. 2, but true lines will arise again, and we will reliably detect them by averaging multiple experiments.

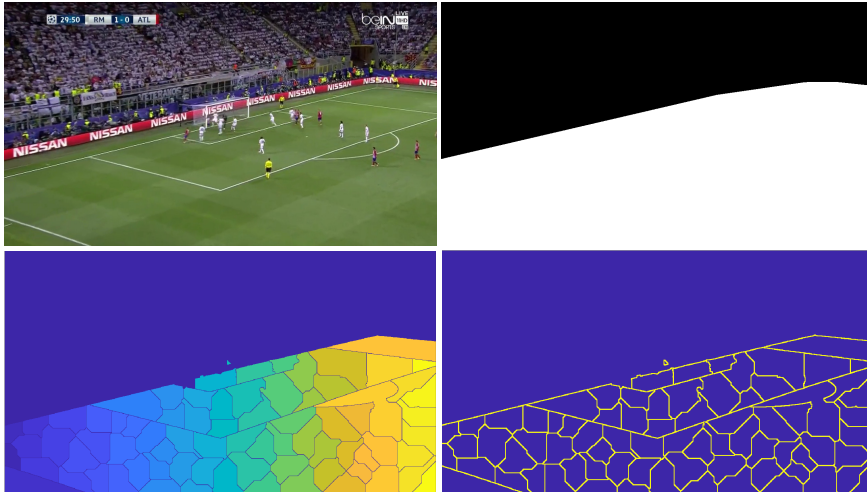


Figure 3: Left to right, top to bottom: original image,  $I$ ; field of play mask,  $M_{PF}$ ; regions determined by a single experiment of stochastic watershed segmentation; corresponding boundaries.

Fig. 3 shows an example of a single experiment whose results clearly exhibit most of the line markings we are looking for, where even lines interrupted by players (e.g., the penalty arc) are present at both sides of the interruption.

Let  $I_{GS}$  be the grayscale image to segment (obtained as described in section 3.1), with a resolution of  $H$  rows and  $W$  columns. A possible first approach is to simply generate sets of  $N$  seeds uniformly distributed across the image:

$$S_i = \left\{ \mathbf{s}_{i,j} = \begin{bmatrix} r_{i,j} \\ c_{i,j} \end{bmatrix} : \begin{array}{l} r_{i,j} = \mathcal{U}(1, H), \\ c_{i,j} = \mathcal{U}(1, W), \\ j \in \{1, 2, \dots, N\} \end{array} \right\}, \quad (1)$$

where  $r$  and  $c$  are the row and column coordinates where each seed  $\mathbf{s}$  is placed, and  $i$  identifies each individual watershed experiment; let us notate the standard seeded watershed transform on a grayscale image  $I_{GS}$  with the set of seeds  $S$  as  $\text{SeededWS}(I_{GS}, S)$ , yielding a binary image where the pixels corresponding to watershed lines are set to 1 and all others are set to 0. Thus, we can compute

$$I_{RWS} = \frac{1}{M} \sum_{i=1}^M \text{SeededWS}(I_{GS}, S_i), \quad (2)$$

where  $M$  is the number of experiments. We can interpret the value of each pixel of  $I_{\text{RWS}}$  as akin to the probability of it being a true watershed line of  $I_{\text{GS}}$ . Since we are interested in robust line detection, the final boundary mask  $M_{\text{B}}$  will only consider as positive detection pixels with values exceeding a threshold  $T_{\text{RWS}}$ <sup>2</sup> and located within a region of interest, in our case the playing field, denoted as  $M_{\text{PF}}$ <sup>3</sup>:

$$M_{\text{B}}(r, c) = \begin{cases} 1, & I_{\text{RWS}}(r, c) \geq T_{\text{RWS}} \wedge M_{\text{PF}}(r, c) = 1; \\ 0, & I_{\text{RWS}}(r, c) < T_{\text{RWS}} \vee M_{\text{PF}}(r, c) = 0. \end{cases} \quad (3)$$

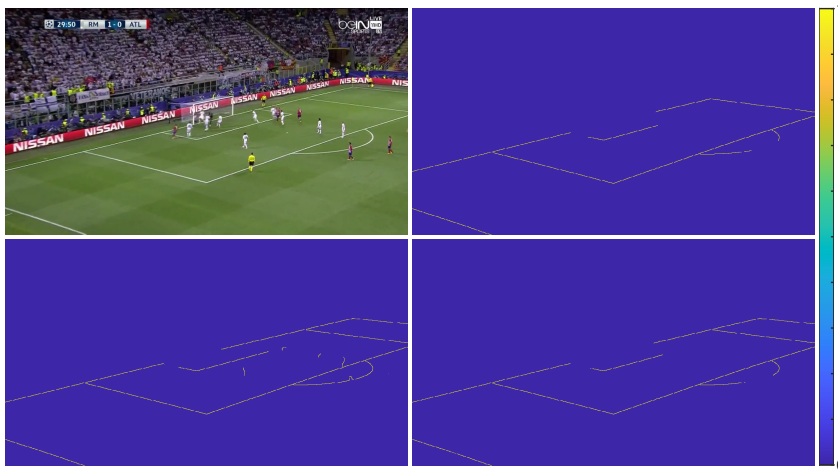


Figure 4: Results applying stochastic watershed with uniform seed distribution for different numbers of seeds and experiments. Top left: original input; top right: few experiments and few seeds ( $M = 20, N = 200$ ); bottom left: few experiments and many seeds ( $M = 20, N = 1000$ ); bottom right: many experiments and few seeds ( $M = 200, N = 200$ ).

However, distributing seeds uniformly across both rows and columns does not guarantee that every region of the image is covered, as Fig. 4 shows: using a relatively small number of seeds has a non-negligible chance of leaving regions uncovered, leading to misdetections. Line misdetection can be solved either increasing the number of seeds or the number of experiments, but the former increases false detections and, while the latter does produce correct results, it does so at significantly higher cost.

To deal with these problems, we propose a windowed random seed generation which will ensure that all the regions of the image contain seeds, attaining quick convergence without increasing the rate of false detections. Let us divide the input image  $I_{\text{GS}}$  into a lattice of  $N_{\text{r}}$  vertical divisions and  $N_{\text{c}}$  horizontal divisions that will delimit  $N_{\text{r}} \times N_{\text{c}}$  non-overlapping rectangular regions (w.l.o.g., let us assume  $H$  and  $W$  are divisible by  $N_{\text{r}}$  and  $N_{\text{c}}$  respectively

<sup>2</sup>We have used  $T_{\text{RWS}} = 0.8$  throughout all the reported experiments to guarantee a robust detection, but it is not a sensitive parameter, the results are very similar for a wide range of values around the chosen one.

<sup>3</sup>There are many available methods to segment the playing field, i.e., the area covered by grass, in the image, namely [32].

to simplify notation); then we will place a single seed with uniform distribution into each of these regions. Thus, we replace equation 1 with

$$S_i = \left\{ \mathbf{s}_{i,j,k} = \begin{bmatrix} r_{i,j,k} \\ c_{i,j,k} \end{bmatrix} : \begin{array}{l} r_{i,j,k} = 1 + \text{mod} \left( r_{o,i} + \frac{jH}{N_r} + \mathcal{U} \left( 1, \frac{H}{N_r} \right), H \right), \\ c_{i,j,k} = 1 + \text{mod} \left( c_{o,i} + \frac{kW}{N_c} + \mathcal{U} \left( 1, \frac{W}{N_c} \right), W \right), \\ r_{o,i} = \mathcal{U} \left( 1, \frac{H}{N_r} \right), \quad c_{o,i} = \mathcal{U} \left( 1, \frac{W}{N_c} \right), \\ j \in \{0, 1, \dots, N_r - 1\}, \quad k \in \{0, 1, \dots, N_c - 1\}, \end{array} \right\}, \quad (4)$$

the rest of the procedure unchanged. Fig. 5 shows the results of this seeding method, where we can see that a small number of experiments ( $M = 20$ ) already yields results comparable to those obtained with the uniform seed generator for  $M = 200$  (shown on Fig. 4). Furthermore, we can also see that increasing significantly the number of experiments does not yield significant advantages. If the lattice used to generate seeds has the same origin in every experiment (e.g.,  $r_{o,i} = c_{o,i} = 0$ ), the procedure yields results which exhibit a faint yet definite pattern, roughly shaped like the lattice, in flat areas of  $I_{GS}$ , as illustrated in Fig. 5; although this effect does not actually affect results, it is easy to eliminate by using a different random origin for the lattice in each experiment, as proposed.

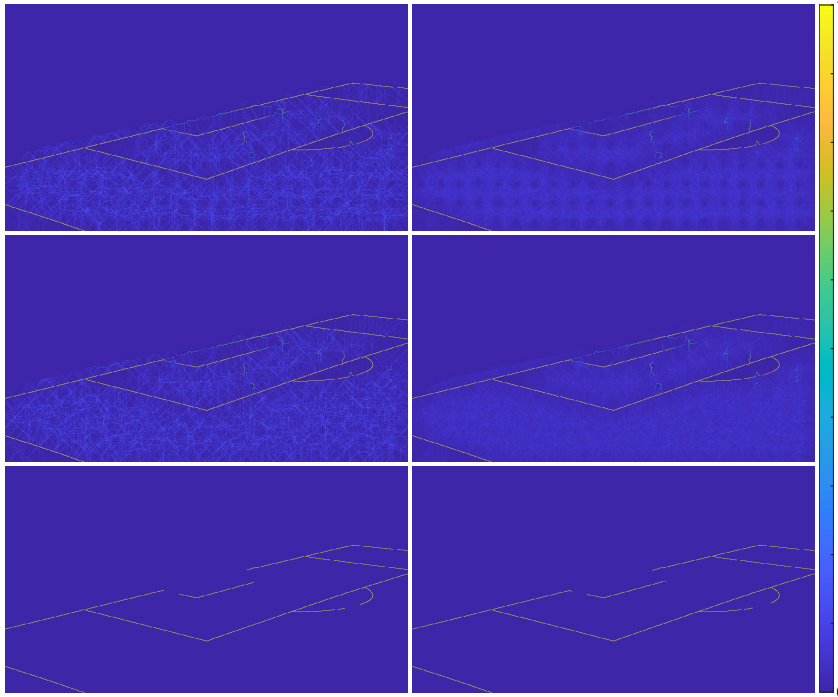


Figure 5: Results applying stochastic watershed with windowed random seed generation. On the left,  $M = 20$ ; on the right,  $M = 200$ . Rows: fixed lattice across experiments (top), proposed approach with different origin in each experiment (middle) and proposed approach after thresholding (bottom).

The proposed seed location algorithm guarantees a bounded distance between seeds, like the iterative Poisson disk sampling [33], but it has a substantially lower cost and is more

amenable to parallelization.

### 3.1. Preprocessing

As explained before, it should reasonably be possible to use the brightness of the RGB input image  $I$  as the input  $I_{GS}$  for the line detection stage because the line markings have a higher brightness than their surroundings. However, in practice, this results in many false line detections due to playing field texture and capture noise. Therefore, before applying the watershed-based line detection we apply a simple pre-processing stage to enhance the input image and maximize the contrast of the white lines against the grass.



Figure 6: Example of false contours due to abrupt illumination changes when performing a local thresholding operation (only the contours inside the pitch area are shown).

A simple solution is to apply a local thresholding operator [34] to remove the noisy areas before applying the line detection stage. However, in the face of abrupt illumination changes this approach is less than ideal because it may create false contours, which will then be erroneously detected as lines (see Fig. 6). To only preserve thin areas that are lighter than their surroundings in all directions, we use the Top-Hat transform [35]:  $X_{TH} = X - X \circ e_{sd}$ , where  $X$  is a grayscale image,  $\circ$  denotes the opening morphological operation and  $e_{sd}$  is a structuring element whose diameter must be slightly greater than the maximum width of the features to be preserved (line marks in our case<sup>4</sup>). The grayscale image to apply the Top-Hat transform onto could just be the luminance of  $I$ , but since the line markings are white, we profit from the fact that they must stand out in each of the R, G and B channels of  $I$ . Thus, we use  $I_{GS} = \min(R_{TH}, G_{TH}, B_{TH})$ , so that non-white features are discarded.

## 4. Classification of line marks

The last stage of our strategy is in charge of determining which of the primitive structures in the playing field (straight line or ellipse) the detected line points belong to. For this, we have developed a procedure based on the adjustment of the detected line points to both types of primitive structures, which consists in the following steps:

---

<sup>4</sup>In the images of the database we have used to assess the quality of the strategy (see Section 5) the width of the lines is typically under 10 pixels. Therefore, a structuring element with a diameter of 11 pixels has been used.



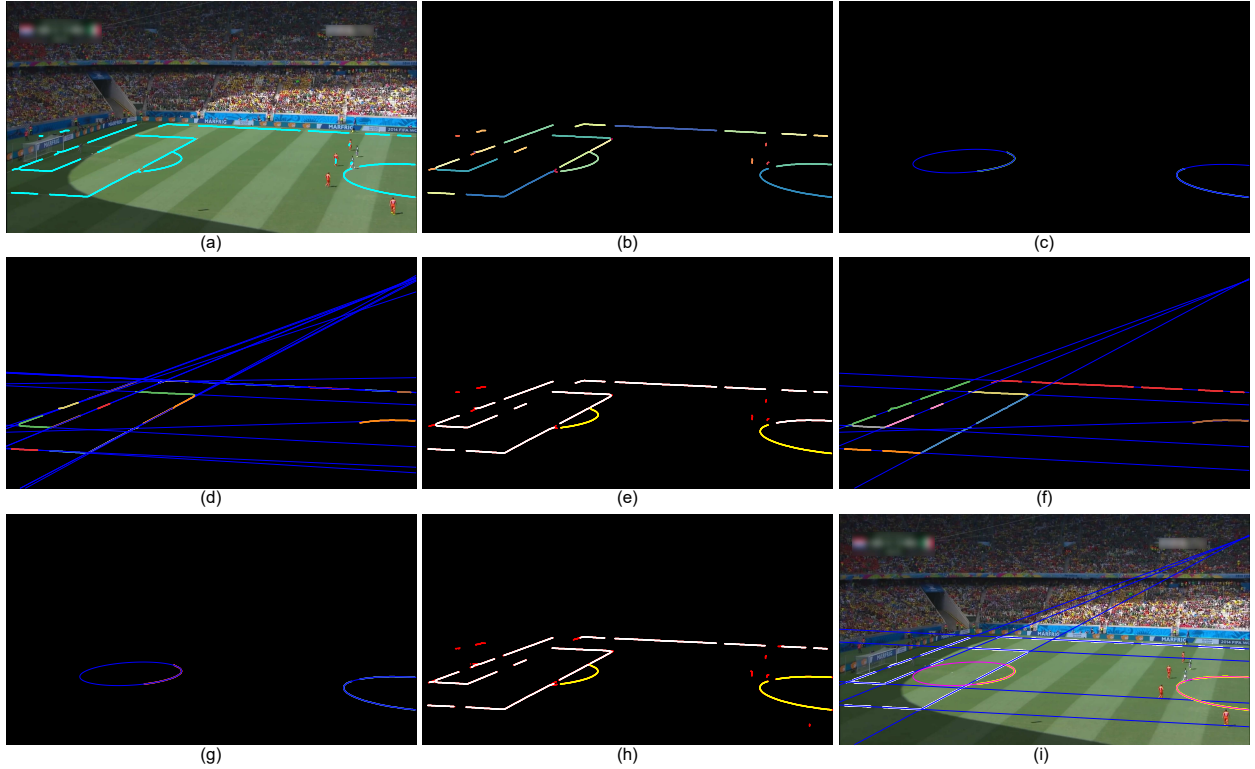


Figure 7: (a) Original image with detected line points in cyan. (b) Connected regions (one different color per region). (c) Ellipses obtained in the initial classification. (d) Straight lines obtained in the initial classification. (e) Initial classification: regions associated to ellipses in yellow, regions associated to straight lines in white, and discarded regions in red. (f) Straight lines and regions after the straight line merging step (the same color for regions associated with the same straight line). (g) Ellipses and regions after the ellipse merging step. (h) Final classification: regions associated to ellipses in yellow, regions associated to straight lines in white, and discarded regions in red. (i) Final straight lines with their associated regions in white and final ellipses with their corresponding regions in yellow.

1. Line point segmentation: The line points in  $M_B$  are segmented into the set of  $N_R$  connected regions,  $R = \{r_i\}_{i=1}^{N_R}$ , that results after removing line intersections (i.e., line points with more than two neighbors). As an example, Fig. 7 shows an image with the line points in  $M_B$  (Fig. 7.a) that has resulted in the set of  $N_R = 26$  connected regions in Fig. 7.b.
2. Initial classification: Each region in  $R$  is classified as part of an ellipse or part of one or more straight lines.
  - (a) The least squares fitting algorithm in [36] is applied to obtain the ellipse that best fits each connected region. The root mean square error (RMSE) of this fit is used as a measure of quality of the fit.
  - (b) Deming regression [37] is used to obtain the straight line that best fits each connected region. If this fit is not accurate enough, the region is divided into the smallest set of subregions that allows an accurate fit to a straight line of each of these subregions. Given that regions corresponding to straight lines tend to be noisy,

we have decided that a fit is accurate enough when the RMSE of the fit is lower than 2.

- (c) Each region or subregion is associated with the primitive structure (ellipse or line) that fits best (i.e., the one with the smallest RMSE).

Smaller regions (e.g., fewer than 50 pixels) are not representative enough by themselves. Therefore, they are initially left unassigned to either primitive structure type.

In the example of Fig. 7 it can be seen that after applying this stage, 2 regions associated with ellipses (Fig. 7.c) and 18 regions associated with straight lines (Fig. 7.d) have been obtained. In addition, in Fig. 7.e it can be seen that 9 regions have been left unassigned (those depicted in red). Therefore, in this example we have gone from 26 to 29 regions, since 3 of the regions have been split to fit two straight lines each.

3. Straight line merging: Regions associated with straight lines are merged which, after merging, still result in a fine fit. Here, since there may be lines represented by segments that practically cross the image, to deal with radial distortion, it has been decided to relax the criterion by which it is determined if a fit is accurate enough, allowing a maximum RMSE of 4 px. In this merging step, the small regions discarded in the previous step are also considered. As it can be seen in Fig. 7.f, after applying this step, we have gone from 18 regions represented by 18 lines to 21 regions represented by 8 lines (3 of the previously discarded regions have been incorporated).
4. Ellipse merging: Regions associated with ellipses are merged if they still result in a good fit together (the RMSE resulting from the fit is at most 4). In this step, the possible fusion with regions previously discarded due to their size is also considered. Notably, not only unassigned or elliptic regions are considered in this step, but also regions hitherto thought of as straights are considered because the curvature of ellipses varies so much that parts of them may locally fit a straight line (for example, the region corresponding to the top of the central circle in the example in Fig. 7) and it is only possible to determine their correspondence with elliptical structures when multiple regions are considered together. Fig. 7.g shows that after applying this step, the mentioned region has been associated with the ellipse corresponding to the central circle of the playing field.
5. Refinement: Ellipses and straight lines are refined by removing pixels that deviate significantly from the estimated models. The criterion used to determine which data fit well is the same as those used in steps 3 and 4 to perform region merging (i.e., the distance to the model is greater than 4). Fig. 7.h, shows the final classification of the line points in  $M_B$ . Thanks to this last stage, small segments that do not actually belong to the geometric model have been discarded (for example, the leftmost piece of the set of regions associated with the upper touchline).

The result in Fig. 7.i shows that the proposed strategy has correctly classified most of the line points detected in the previous stage into their corresponding ellipses (central circle and arc of the left area) and straight lines. This image also shows that 7 of the 8 straight lines have been correctly modeled; the only misdetection, due to its small size in this image, occurs on the upper line of the goal area.

## 5. Results

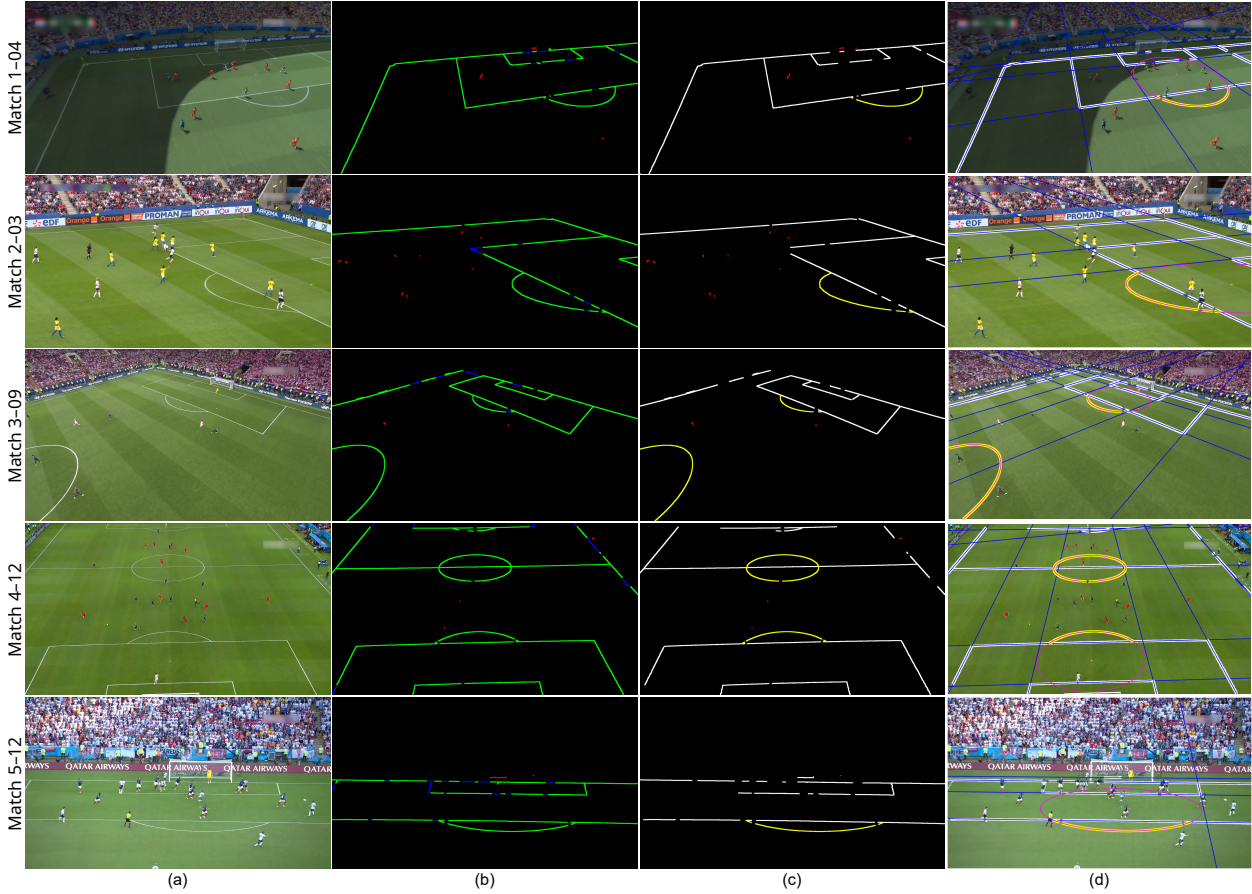


Figure 8: Some representative results obtained in the test sequences. (a) Original images. (b) Line mark segmentation: true positives in green, false negatives in blue, and false positives in red. (c) Line mark classification: in white the points assigned to straight lines, in yellow the points assigned to elliptical lines, and in red the discarded points. (d) Primitives: straight lines in blue, regions associated to straight lines in white, ellipses in purple, regions associated to ellipses in yellow.

To assess the quality of the proposed strategy, we have created a new and public database named LaSoDa<sup>5</sup>. As far as we know, there is only one other database that, like ours, allows the evaluation of the quality of algorithms to detect or segment line marks in images of soccer matches [24]. However, this database presents two serious shortcomings: all its images have been acquired from the same viewpoint and similar wide-view angle, limiting the variety of its contents; and, crucially, many of the homography matrices provided in this database are too inaccurate to provide a good registration of a model of the pitch with the images, precluding a pixel-level evaluation of line mark detections.

LaSoDa is composed by 60 annotated images from matches in five stadiums with different characteristics (e.g., positions of the cameras, view angles, grass colors) and light conditions

<sup>5</sup><http://www.gti.ssr.upm.es/data/>

(day and night). Its images cover all areas of the playing field, show five different zoom levels—from 1 (closest zoom) to 5 (widest zoom)—, have been acquired with four different types of cameras—master camera (MC), side camera (SC), end camera (EC), and aerial camera (AC)—, and include different and challenging lighting conditions (e.g., day and night matches, and some heavily shaded images).

The quality of the results has been measured by the recall (rec), precision (pre), and F-score ( $F$ ) metrics, which are computed as:

$$\text{rec} = \frac{\text{tp}}{\text{tp} + \text{fn}}, \text{pre} = \frac{\text{tp}}{\text{tp} + \text{fp}}, F = \frac{2\text{tp}}{2\text{tp} + \text{fp} + \text{fn}}, \quad (5)$$

where tp, fn, and fp are, respectively, the amounts of true positives, false negatives and false positives.

Table 1: Results at pixel and object level

Image Id.	Camera Type	Zoom level	Segmentation			Classification (px)						Classification (obj)					
			rec	pre	F	Straight			Elliptical			Straight			Elliptical		
						rec	pre	F	rec	pre	F	rec	pre	F	rec	pre	F
1-01	MC	2	0.90	0.99	0.94	0.78	1.00	0.88	1.00	1.00	1.00	0.75	1.00	0.86	1.00	1.00	1.00
1-02	MC	4	0.94	0.98	0.96	0.89	1.00	0.94	0.96	1.00	0.98	1.00	1.00	1.00	1.00	1.00	1.00
1-03	EC	1	0.93	1.00	0.96	0.81	1.00	0.90	0.85	1.00	0.92	0.75	0.82	0.78	0.67	1.00	0.80
1-04	AC	3	0.97	1.00	0.99	0.95	1.00	0.98	1.00	1.00	1.00	1.00	1.00	1.00	1.00	1.00	1.00
1-05	MC	4	0.99	0.97	0.98	0.98	1.00	0.99	-	-	-	1.00	1.00	1.00	-	-	-
1-06	MC	2	0.87	0.99	0.93	0.78	1.00	0.87	0.98	1.00	0.99	1.00	0.83	0.91	1.00	1.00	1.00
1-07	MC	5	0.89	1.00	0.94	0.84	0.94	0.89	0.00	1.00	0.00	1.00	0.78	0.88	0.00	1.00	0.00
1-08	MC	3	0.96	0.99	0.97	0.95	1.00	0.97	-	-	-	1.00	1.00	1.00	-	-	-
1-09	MC	3	0.97	1.00	0.98	0.96	1.00	0.98	0.76	1.00	0.86	1.00	1.00	1.00	1.00	1.00	1.00
1-10	SC	3	0.92	0.99	0.95	0.89	1.00	0.94	1.00	1.00	1.00	1.00	1.00	1.00	1.00	1.00	1.00
1-11	AC	3	1.00	1.00	1.00	0.98	1.00	0.99	0.99	1.00	1.00	1.00	1.00	1.00	1.00	1.00	1.00
1-12	MC	4	0.94	1.00	0.97	0.89	1.00	0.94	0.95	1.00	0.98	1.00	0.86	0.92	1.00	1.00	1.00
2-01	MC	3	0.97	0.98	0.98	0.91	0.96	0.93	1.00	1.00	1.00	1.00	1.00	1.00	1.00	1.00	1.00
2-02	MC	3	0.96	0.99	0.98	0.94	0.96	0.95	0.00	1.00	0.00	1.00	0.80	0.89	0.00	1.00	0.00
2-03	MC	3	0.97	0.99	0.98	0.95	1.00	0.97	0.99	1.00	1.00	1.00	0.86	0.92	1.00	1.00	1.00
2-04	EC	4	0.98	0.98	0.98	0.97	1.00	0.98	0.97	1.00	0.98	1.00	1.00	1.00	1.00	1.00	1.00
2-05	SC	3	0.99	0.99	0.99	0.98	0.99	0.99	0.96	1.00	0.98	1.00	0.90	0.95	1.00	1.00	1.00
2-06	SC	3	0.98	0.99	0.99	0.97	1.00	0.98	0.98	1.00	0.99	1.00	1.00	1.00	1.00	1.00	1.00
2-07	MC	3	0.93	1.00	0.96	0.90	1.00	0.95	0.94	1.00	0.97	1.00	0.67	0.80	1.00	1.00	1.00
2-08	MC	2	0.95	0.99	0.97	0.96	0.96	0.96	0.00	1.00	0.00	1.00	0.80	0.89	0.00	1.00	0.00
2-09	SC	5	0.82	0.97	0.89	0.79	1.00	0.88	-	-	-	1.00	0.83	0.91	-	-	-
2-10	SC	5	0.76	0.97	0.85	0.70	1.00	0.83	-	-	-	1.00	0.71	0.83	-	-	-
2-11	EC	4	0.97	0.99	0.98	0.94	0.88	0.91	0.58	1.00	0.73	0.67	0.44	0.53	0.50	1.00	0.67
2-12	SC	1	0.96	0.97	0.97	0.93	0.97	0.95	0.94	1.00	0.97	1.00	1.00	1.00	1.00	1.00	1.00
3-01	EC	1	0.93	0.98	0.95	0.91	0.99	0.95	0.96	1.00	0.98	1.00	0.75	0.86	1.00	1.00	1.00
3-02	MC	2	0.99	0.99	0.99	0.97	1.00	0.99	1.00	1.00	1.00	1.00	0.90	0.95	1.00	1.00	1.00
3-03	MC	4	0.97	1.00	0.98	0.93	1.00	0.97	-	-	-	1.00	1.00	1.00	-	-	-

Image Id.	Camera Type	Zoom level	Segmentation			Classification (px)						Classification (obj)					
			rec	pre	F	Straight			Elliptical			Straight			Elliptical		
						rec	pre	F	rec	pre	F	rec	pre	F	rec	pre	F
3-04	MC	5	0.94	1.00	0.97	0.91	0.92	0.92	0.00	1.00	0.00	1.00	0.89	0.94	0.00	1.00	0.00
3-05	MC	1	0.99	0.99	0.99	0.99	1.00	1.00	0.99	1.00	0.99	1.00	1.00	1.00	1.00	1.00	1.00
3-06	MC	4	0.95	0.98	0.96	0.94	1.00	0.97	0.94	1.00	0.97	1.00	1.00	1.00	1.00	1.00	1.00
3-07	AC	3	1.00	1.00	1.00	0.96	1.00	0.98	1.00	1.00	1.00	1.00	0.73	0.84	1.00	1.00	1.00
3-08	MC	1	0.99	0.99	0.99	0.99	1.00	1.00	0.96	1.00	0.98	1.00	1.00	1.00	1.00	1.00	1.00
3-09	AC	1	1.00	1.00	1.00	1.00	1.00	1.00	0.98	1.00	0.99	1.00	0.89	0.94	1.00	1.00	1.00
3-10	SC	5	0.97	0.99	0.98	0.95	0.96	0.96	0.00	1.00	0.00	1.00	0.82	0.90	0.00	1.00	0.00
3-11	AC	4	0.98	1.00	0.99	0.97	1.00	0.98	0.95	1.00	0.97	1.00	1.00	1.00	1.00	1.00	1.00
3-12	AC	1	0.98	1.00	0.99	0.97	1.00	0.98	0.99	1.00	0.99	0.78	1.00	0.88	1.00	1.00	1.00
4-01	AC	1	0.99	1.00	1.00	0.99	0.95	0.97	0.74	1.00	0.85	0.78	0.78	0.78	0.50	1.00	0.67
4-02	AC	3	1.00	1.00	1.00	0.99	1.00	1.00	1.00	1.00	1.00	1.00	1.00	1.00	1.00	1.00	1.00
4-03	AC	3	0.99	1.00	0.99	0.99	1.00	0.99	1.00	1.00	1.00	1.00	1.00	1.00	1.00	1.00	1.00
4-04	SC	3	0.94	0.99	0.96	0.93	1.00	0.96	0.90	1.00	0.95	1.00	0.89	0.94	1.00	1.00	1.00
4-05	AC	3	0.98	0.99	0.99	0.97	1.00	0.98	0.99	1.00	1.00	1.00	1.00	1.00	1.00	1.00	1.00
4-06	SC	2	0.98	0.99	0.99	0.97	1.00	0.98	0.97	1.00	0.99	0.80	1.00	0.89	1.00	1.00	1.00
4-07	MC	3	0.99	1.00	0.99	0.94	1.00	0.97	0.97	1.00	0.99	1.00	1.00	1.00	1.00	1.00	1.00
4-08	AC	4	0.94	1.00	0.97	0.96	0.98	0.97	0.00	1.00	0.00	1.00	0.67	0.80	0.00	1.00	0.00
4-09	AC	1	0.95	0.96	0.95	0.92	0.98	0.95	0.99	1.00	1.00	1.00	0.73	0.84	1.00	1.00	1.00
4-10	AC	3	1.00	1.00	1.00	0.98	1.00	0.99	1.00	1.00	1.00	0.86	1.00	0.92	1.00	1.00	1.00
4-11	MC	2	0.98	1.00	0.99	0.98	1.00	0.99	0.96	1.00	0.98	1.00	0.89	0.94	1.00	1.00	1.00
4-12	AC	1	0.99	0.99	0.99	0.97	0.98	0.98	0.85	1.00	0.92	1.00	0.91	0.95	0.67	1.00	0.80
5-01	MC	2	0.99	0.99	0.99	0.99	1.00	0.99	0.95	1.00	0.97	1.00	1.00	1.00	1.00	1.00	1.00
5-02	MC	3	0.95	1.00	0.98	0.93	1.00	0.96	0.96	1.00	0.98	1.00	1.00	1.00	1.00	1.00	1.00
5-03	MC	3	0.98	0.98	0.98	0.97	1.00	0.98	0.96	0.99	0.97	1.00	1.00	1.00	1.00	1.00	1.00
5-04	AC	3	0.99	1.00	0.99	0.98	1.00	0.99	0.99	1.00	0.99	1.00	1.00	1.00	1.00	1.00	1.00
5-05	AC	5	0.99	1.00	1.00	0.99	1.00	1.00	-	-	-	1.00	1.00	1.00	-	-	-
5-06	MC	5	0.89	1.00	0.94	0.86	1.00	0.92	-	-	-	0.80	0.80	0.80	-	-	-
5-07	SC	5	0.78	0.99	0.87	0.75	0.99	0.85	0.00	1.00	0.00	0.71	0.83	0.77	0.00	1.00	0.00
5-08	AC	5	0.80	0.99	0.89	0.74	1.00	0.85	0.82	0.97	0.89	0.71	0.83	0.77	1.00	1.00	1.00
5-09	SC	4	0.90	1.00	0.94	0.90	1.00	0.95	0.54	1.00	0.70	1.00	0.89	0.94	1.00	1.00	1.00
5-10	SC	3	0.88	1.00	0.93	0.87	1.00	0.93	0.57	1.00	0.72	1.00	1.00	1.00	1.00	1.00	1.00
5-11	AC	1	0.97	0.99	0.98	0.95	1.00	0.97	0.95	1.00	0.97	1.00	1.00	1.00	1.00	1.00	1.00
5-12	AC	4	0.93	1.00	0.97	0.91	1.00	0.95	1.00	1.00	1.00	0.67	1.00	0.80	1.00	1.00	1.00
Match 1			0.94	0.99	0.96	0.89	0.99	0.94	0.92	1.00	0.96	0.94	0.93	0.93	0.86	1.00	0.92
Match 2			0.95	0.99	0.97	0.92	0.97	0.94	0.82	1.00	0.90	0.97	0.81	0.88	0.77	1.00	0.87
Match 3			0.97	0.99	0.98	0.96	0.99	0.97	0.89	1.00	0.94	0.98	0.89	0.93	0.88	1.00	0.93
Match 4			0.98	0.99	0.98	0.97	0.99	0.98	0.89	1.00	0.94	0.95	0.88	0.92	0.81	1.00	0.90
Match 5			0.92	0.99	0.96	0.90	1.00	0.94	0.89	1.00	0.94	0.91	0.94	0.92	0.92	1.00	0.96
Total			0.95	0.99	0.97	0.93	0.99	0.96	0.88	1.00	0.93	0.95	0.89	0.92	0.85	1.00	0.92

Table 1 summarizes the quality measures obtained in each of the images in the proposed database using the provided ground truth for the mask of the playing field  $M_{PF}$ , as well as the overall quality results for each match individually and for the entire database. In

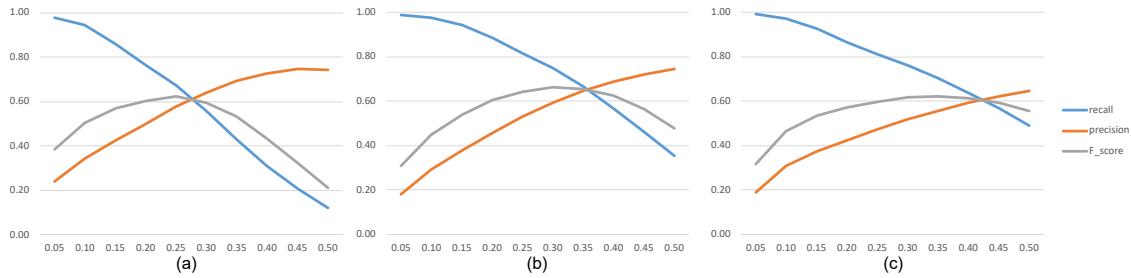


Figure 9: Global quality results obtained with other state-of-the-art line mark segmentation algorithms: (a) Top-Hat transform, (b) Sobel edge detector, and (c) LoG edge detector.

addition, Fig. 8 shows the results of a significant image in each of the five matches in the database (the results corresponding to the rest of the images are available on the LaSoDa website).

The “Segmentation” columns of Table 1 report the pixel-level results of the segmentation of the line marks in bulk (i.e., before classification into straight or elliptical marks). These results show that the quality of the line mark segmentation is very high, with F-score values over 0.9 in most images and over 0.8 in the remaining few, yielding an overall F-score of 0.97. The few false positives are mainly due to players wearing white kits and to white elements of the goals, which show a similar appearance to that of the white lines on the pitch. False negatives correspond to line points occluded by players or that barely stand out from the grass because they are very far from the camera.

To compare with the most commonly used methods for line detection, Fig. 9 summarizes the global quality results obtained with three of the most popular algorithms that are used in other works, as indicated in section 2, to highlight the line markings in soccer images: the Sobel edge detector, the LoG edge detector, and the Top-Hat transform. We can see that none of them performs well across the whole dataset: there is no threshold value that gives a really good balance between precision and recall in any of these methods. Fig. 10 compares the results obtained on an image where approximately half of the playing field is strongly sunlit, while the other half is in shadow. It can be seen that only our strategy is able to detect the line marks in all areas of the playing field, while at the same time yielding the fewest false positives.

The “Classification (px)” columns of Table 1 also report pixel-wise results, but after classification into straight and elliptical lines, showing that after applying the line mark classification stage the quality obtained is very high too. As it can be seen in Fig. 8 and in the table, most false detections that resulted from the segmentation stage have been discarded. However, some of the correctly segmented points at this stage have also been discarded, not being assigned to straight lines or ellipses, which has caused a slight decrease in the recall. This generally occurs with line segments that, because of their small size, have not been conclusively classified as any of the primitive structures.

Finally, the “Classification (obj)” columns of Table 1 report the object-level results corresponding to the primitive structures associated with the line points resulting from the classification (illustrated in the last column of Fig. 8). Out of the 402 straight lines featured

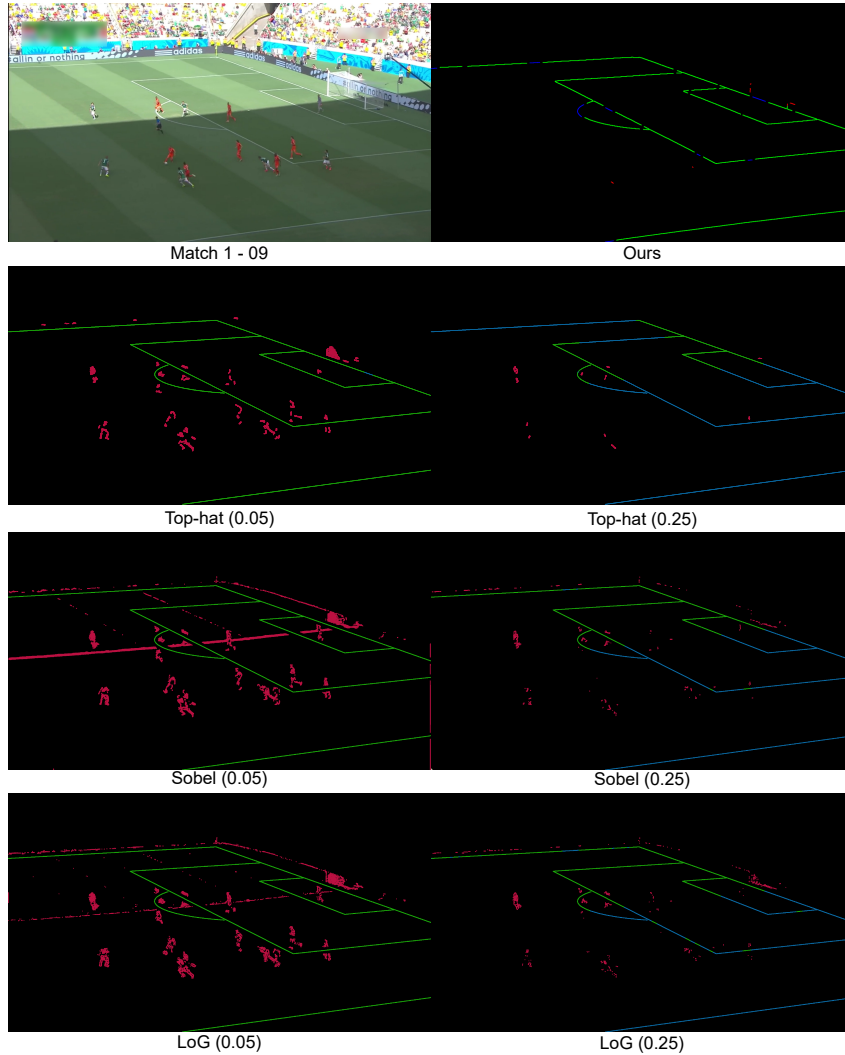


Figure 10: Example of line mark segmentation with the considered algorithms with different normalized threshold values: true positives in green, false negatives in blue, and false positives in red.

in the whole of the database, only 22 have been misdetections. These non-detections are associated with the shortest line segments, as illustrated in Fig. 8. On the other hand, 59 false detections have been obtained, which are overwhelmingly due to cases where only the straightest parts of ellipses (mainly on the penalty arc, which is small and frequently presents partial occlusion from players) are visible and have been wrongly classified as small straight lines. Regarding ellipses, out of the 71 that appear in the 60 images analyzed, 12 have been misdetections but there are no false detections at all. These non-detections are associated with images where the detected line segments have not been long enough to determine that they fit an ellipse better than a straight line (an example of this can also be seen in the last of the images in Fig. 8).

Figure 11 reports the global results using the Hough transform, a very popular method

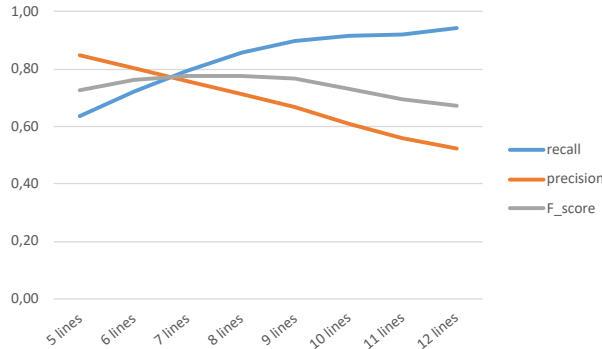


Figure 11: Straight line detection results obtained with the Hough transform.

for straight line detection in the methods reviewed in section 2, from the points in  $M_B$ . As already stated in section 2, this method requires the user to set a target number of lines to search for. These results show that setting a low number of target lines results in many misdetections; conversely, a high number of target lines results in a significant increase in the number of false detections. The best result has been obtained by configuring the method to obtain 8 lines per image. However, this global optimal configuration still results in a relatively low F-score of 0.78, while our proposal reaches 0.90.

## 6. Conclusions

We have presented a novel strategy to segment and classify line markings in football pitches, irrespectively of camera position or orientation, and validated its effectiveness on a variety of images from several stadiums. This strategy is based on the stochastic watershed transform, which is usually employed to segment regions rather than lines, but we have shown that, coupled with the seeding strategy we propose, it provides a robust way to segment the line markings from the playing field without assuming that the lines are straight or conform to any particular pattern. Specifically, our method is able to correctly segment the curved lines that are typical of wide-angle takes due to radial distortion of broadcasting cameras or cope with the interference of players or the ball, which frequently cause errors in most methods based on the Hough transform. Following the segmentation of the lines, we have also proposed a simple method to classify the segmented pixels into straight lines and ellipses or parts thereof. This method is also robust against moderate radial distortion and outliers, and does not make assumptions about the viewpoint or the distribution of the markings, leaving those considerations for later higher-level classification and camera resection stages.

To assess the quality of the proposed strategy, a new and public database (LaSoDa) has been developed. LaSoDa is composed of 60 annotated images from matches in stadiums with different characteristics (positions of the cameras, grass colors) and light conditions (natural and artificial).

Some improvements can be considered for future work, for instance parallelization of the watershed transform, since the regular arrangement of seeds may allow to independently



compute different regions of the image, but the current proposal already constitutes a solid foundation for other stages in a sports video analysis pipeline to build upon.

## Acknowledgments

This work has been partially supported by MCIN/AEI/10.13039/501100011033 of the Spanish Government [grant number PID2020-115132RB (SARAOS)].

## References

- [1] L. G. S. Félix, C. M. Barbosa, I. A. Carvalho, V. da F. Vieira, C. R. Xavier, Forecasting soccer market tendencies using link prediction, in: O. Gervasi, B. Murgante, S. Misra, C. Garau, I. Blečić, D. Taniar, B. O. Apduhan, A. M. A. C. Rocha, E. Tarantino, C. M. Torre, Y. Karaca (Eds.), *Computational Science and Its Applications – ICCSA 2020*, Springer International Publishing, Cham, 2020, pp. 663–675.
- [2] D. T. Kirkendall, Evolution of soccer as a research topic, *Progress in Cardiovascular Diseases* 63 (6) (2020) 723–729.
- [3] C. Goebert, G. P. Greenhalgh, A new reality: Fan perceptions of augmented reality readiness in sport marketing, *Computers in Human Behavior* 106 (2020) 106231.
- [4] G. Andrienko, N. Andrienko, G. Anzer, P. Bauer, G. Budziak, G. Fuchs, D. Hecker, H. Weber, S. Wrobel, Constructing spaces and times for tactical analysis in football, *IEEE transactions on visualization and computer graphics* 27 (4) (2021) 2280–2297.
- [5] R. Kapela, A. Świetlicka, A. Rybarczyk, K. Kolanowski, et al., Real-time event classification in field sport videos, *Signal Processing: Image Communication* 35 (2015) 35–45.
- [6] C. Cuevas, D. Quilón, N. García, Automatic soccer field of play registration, *Pattern Recognition* (2020) 107278.
- [7] J. Chen, F. Zhu, J. J. Little, A two-point method for PTZ camera calibration in sports, in: *IEEE Winter Conference on Applications of Computer Vision (WACV)*, 2018, pp. 287–295.
- [8] L. Citraro, P. Márquez-Neila, S. Savare, V. Jayaram, C. Dubout, F. Renaut, A. Hasfura, H. Ben Shitrit, P. Fua, Real-time camera pose estimation for sports fields, *Machine Vision and Applications* 31 (3) (2020) 1–13.
- [9] Q. Yao, A. Kubota, K. Kawakita, K. Nonaka, H. Sankoh, S. Naito, Fast camera self-calibration for synthesizing free viewpoint soccer video, in: *IEEE International Conference on Acoustics, Speech and Signal Processing (ICASSP)*, 2017, pp. 1612–1616.
- [10] J. Angulo, D. Jeulin, Stochastic watershed segmentation, in: *Proceedings of the International Symposium on Mathematical Morphology*, 2007, pp. 265–276.
- [11] U. Rao, U. C. Pati, A novel algorithm for detection of soccer ball and player, in: *2015 International Conference on Communications and Signal Processing (ICCSP)*, 2015, pp. 0344–0348.
- [12] S. Zhang, Research on effective field lines detection and tracking algorithm in soccer videos, *International Journal of Multimedia and Ubiquitous Engineering* 10 (7) (2015) 75–84.
- [13] C. Direkoglu, M. Sah, N. E. O’Connor, Player detection in field sports, *Machine Vision and Applications* 29 (2) (2018) 187–206.
- [14] F. F. Doria, F. B. Lima, A. K. Sato, R. Y. Takimoto, A. Barari, F. S. Tsuzuki, M. S. Tsuzuki, Soccer field lines determination and 3d reconstruction, in: *International Conference on Geometry and Graphics*, 2021, pp. 568–579.
- [15] F. Szenberg, P. C. P. Carvalho, M. Gattass, Automatic camera calibration for image sequences of a football match, in: *International Conference on Advances in Pattern Recognition*, 2001, pp. 303–312.
- [16] J. Bu, S. Lao, L. Bai, Automatic line mark recognition and its application in camera calibration in soccer video, in: *2011 IEEE International Conference on Multimedia and Expo*, 2011, pp. 1–6.

- [17] L. Sun, G. Liu, Field lines and players detection and recognition in soccer video, in: 2009 IEEE International Conference on Acoustics, Speech and Signal Processing, 2009, pp. 1237–1240.
- [18] Y. Yang, D. Li, Robust player detection and tracking in broadcast soccer video based on enhanced particle filter, *Journal of Visual Communication and Image Representation* 46 (2017) 81–94.
- [19] M. Alemán-Flores, L. Alvarez, L. Gómez, P. Henríquez, L. Mazorra, Camera calibration in sport event scenarios, *Pattern recognition* 47 (1) (2014) 89–95.
- [20] M. M. N. Ali, M. Abdullah-Al-Wadud, S.-L. Lee, An efficient algorithm for detection of soccer ball and players, *Proc. 16th ASTL Control and Networking* 16 (2012) 39–46.
- [21] D. A. Sadlier, N. E. O’Connor, Event detection in field sports video using audio-visual features and a support vector machine, *IEEE Transactions on Circuits and Systems for Video Technology* 15 (10) (2005) 1225–1233.
- [22] I. Jabri, et al., Camera calibration using court models for real-time augmenting soccer scenes, *Multimedia Tools and Applications* 51 (3) (2011) 997–1011.
- [23] J.-B. Hayet, J. H. Piater, J. G. Verly, Fast 2D model-to-image registration using vanishing points for sports video analysis, in: *IEEE International Conference on Image Processing 2005*, Vol. 3, 2005, pp. 417–420.
- [24] N. Homayounfar, S. Fidler, R. Urtasun, Sports field localization via deep structured models, in: *Proceedings of the IEEE Conference on Computer Vision and Pattern Recognition*, 2017, pp. 5212–5220.
- [25] P. Mukhopadhyay, B. B. Chaudhuri, A survey of Hough transform, *Pattern Recognition* 48 (3) (2015) 993–1010.
- [26] L. Xu, E. Oja, P. Kultanen, A new curve detection method: randomized Hough transform (RHT), *Pattern recognition letters* 11 (5) (1990) 331–338.
- [27] J. R. Bergen, H. Shvaytser, A probabilistic algorithm for computing Hough transforms, *Journal of algorithms* 12 (4) (1991) 639–656.
- [28] Y. Wu, H. Wang, F. Tang, Z. Wang, Efficient conic fitting with an analytical Polar-N-Direction geometric distance, *Pattern Recognition* 90 (2019) 415–423.
- [29] K. Wan, L. Joo-Hwee, C. Xu, X. Yu, Real-time camera field-view tracking in soccer video, in: 2003 IEEE International Conference on Acoustics, Speech, and Signal Processing, 2003. *Proceedings.(ICASSP’03)*., Vol. 3, 2003, pp. 185–188.
- [30] F. Malmberg, C. L. Luengo Hendriks, An efficient algorithm for exact evaluation of stochastic watersheds, *Pattern Recognition Letters* 47 (2014) 80–84, *advances in Mathematical Morphology*.
- [31] J. C. Maxwell, On hills and dales, *The London, Edinburgh, and Dublin Philosophical Magazine and Journal of Science* 40 (269) (1870) 421–427.
- [32] D. Quilón, R. Mohedano, C. Cuevas, N. García, Unsupervised high-quality soccer field segmentation, in: *International Symposium on Consumer Electronics (ISCE)*, 2015, pp. 1–2.
- [33] R. Bridson, Fast Poisson disk sampling in arbitrary dimensions, in: *ACM SIGGRAPH 2007 Sketches*, Association for Computing Machinery, New York, NY, USA, 2007, p. 22.
- [34] D. Bradley, G. Roth, Adaptive thresholding using the integral image, *Journal of Graphics Tools* 12 (2) (2007) 13–21.
- [35] F. Meyer, Iterative image transformations for an automatic screening of cervical smears., *Journal of Histochemistry & Cytochemistry* 27 (1) (1979) 128–135.
- [36] A. Fitzgibbon, M. Pilu, R. B. Fisher, Direct least square fitting of ellipses, *IEEE Transactions on pattern analysis and machine intelligence* 21 (5) (1999) 476–480.
- [37] P. J. Cornbleet, N. Gochman, Incorrect least-squares regression coefficients in method-comparison analysis., *Clinical chemistry* 25 (3) (1979) 432–438.